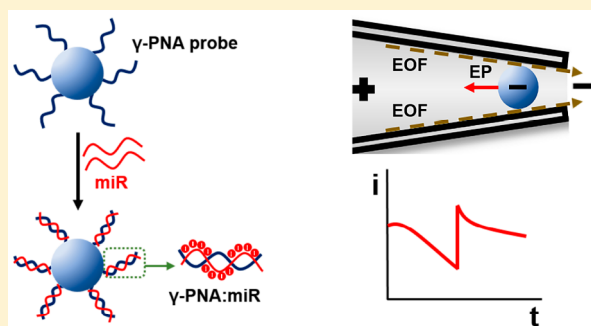


## Sequence-Specific Detection of MicroRNAs Related to Clear Cell Renal Cell Carcinoma at fM Concentration by an Electroosmotically Driven Nanopore-Based Device

Yuqian Zhang,<sup>†</sup> Ankit Rana,<sup>†</sup> Yiwen Stratton,<sup>‡</sup> Maria F. Czyzyk-Krzeska,<sup>‡,§</sup> and Leyla Esfandiari<sup>\*,†,||</sup><sup>†</sup>Department of Electrical Engineering and Computing Systems, University of Cincinnati, Cincinnati, Ohio 45221, United States<sup>‡</sup>Department of Cancer Biology, University of Cincinnati, Cincinnati, Ohio 45267, United States<sup>§</sup>Department of Veterans Affairs, VA Research Service, Cincinnati, Ohio 45220, United States<sup>||</sup>Department of Biomedical Chemical and Environmental Engineering, University of Cincinnati, Cincinnati, Ohio 45221, United States

## S Supporting Information

**ABSTRACT:** MicroRNAs (miRs) are small noncoding RNAs that play a critical role in gene regulation. Recently, traces of cancer-related miRs have been identified in body fluids, which make them remarkable noninvasive biomarkers. In this study, a new nanopore-based detection scheme utilizing a borosilicate micropipette and an assay of complementary  $\gamma$ -peptide nucleic acid ( $\gamma$ -PNA) probes conjugated to polystyrene beads have been reported for the detection of miR-204 and miR-210 related to the clear cell Renal Cell Carcinoma (ccRCC). Electroosmotic flow (EOF) is induced as the driving force to transport PNA-beads harboring target miRs to the tip of the pore (sensing zone), which results in pore blockades with unique and easily distinguishable serrated shape electrical signals. The concentration detection limit is investigated to be 1 and 10 fM for miR-204 and miR-210, respectively. The EOF transport mechanism enables highly sensitive detection of molecules with low surface charge density with 97.6% detection accuracy compared to the conventional electrophoretically driven methods. Furthermore, resistive-pulse experiments are conducted to study the correlation of the particles' surface charge density with their translocation time and verify the detection principle.



One of the significant advancements in molecular biology has been the identification of microRNAs, which are small noncoding RNAs (~20 nt) that regulate various biological phenomena, such as development and homeostasis.<sup>1</sup> In addition, miRs play an important role in carcinogenesis; their unusual expression level, either up-regulated or down-regulated, have been identified to be correlated with disruption of normal biological processes.<sup>2–4</sup> Recently, circulating miRs have been observed in extracellular human body fluids including blood plasma, urine, and saliva as nuclease-resistant circulating entities in both free-floating and microvesicle (exosome) associated states.<sup>5–8</sup> Thus, they have attracted a great deal of attention as noninvasive biomarkers due to ease of access and high stability compared to messenger RNAs (mRNAs) and proteins.<sup>9,10</sup>

Currently, qRT-PCR technology is considered as the “gold standard” for miR detection due to its high sensitivity and specificity.<sup>11–13</sup> However, this technique requires time-consuming and expensive amplification steps along with labeling and enzymatic reactions. Moreover, the design of the primers for small miR sequences has been reported to be challenging.<sup>11,14</sup> New PCR-free biosensor-based technologies such as electrochemical<sup>15–17</sup> and optical sensors<sup>18–20</sup> with concen-

tration detection limits ranging from attomolar (aM) to nanomolar (nM) have been developed for miR analysis.<sup>21</sup> Another straightforward and effective approach for miR detection has been the nanopore-based sensing.<sup>21</sup> Nanopores have gained significant attention in the field of genome sequencing,<sup>22–24</sup> molecular sensing,<sup>25,26</sup> and medical diagnostics<sup>27,28</sup> due to their intrinsic ultrasensitive, PCR-independent, truly reagentless, and rapid detection criteria.<sup>29</sup> Several groups have utilized nanopores as an alternative approach for direct detection of circulating miRs.<sup>30,31</sup> For instance, in a pilot study by Gu and Wang, a protein nanopore and a polycationic peptide-PNA probe were used to selectively discriminate plasma miRs from lung cancer patients and healthy individuals with much lower variability compared to the qRT-PCR.<sup>32</sup> The same group has demonstrated the feasibility of multiple miRs detection in a single protein pore by designing a series of barcode probes to encode different targets along with the click chemistry technique to specifically modulate ionic flow as each

Received: May 22, 2017

Accepted: August 3, 2017

Published: August 23, 2017



probe-miR passes through the pore.<sup>33</sup> Besides protein pores, Wanunu et al. have fabricated a 3 nm diameter pore in a 7 nm thick silicon nitride (SiN) to detect the liver miR hybridized with the probe after enrichment.<sup>34</sup> Although these methods are highly sensitive, they are undesirable as robust systems due to the instability of the lipid bilayer and tedious fabrication procedure of a thin 3 nm pore.

In the work described here, we have demonstrated an electroosmotically driven nanopore-based sensor and an assay of  $\gamma$ -PNA probes conjugated beads to detect two miRs, miR-204 and miR-210, related to ccRCC at fM detection limit. CcRCC is a malignant kidney cancer distinguishable by the early loss of the von Hippel-Lindau tumor suppressor protein (VHL), leading to the accumulation of the hypoxia inducible transcription factor (HIF) and induction of HIF-responsive genes.<sup>35</sup> As a model system, we used human 786-O RCC cell line where the VHL gene is inactivated (VHL<sup>-</sup>) and expresses high levels of miR-210 and low levels of miR-204, and an isogenic cell line with reconstituted VHL (VHL<sup>+</sup>), where levels of miR-210 are decreased and levels of miR-204 are induced.<sup>36–38</sup> The glass micropipette has been chosen as the pore construct since it has shown attractive sensing properties such as low-noise, robustness and relatively simple fabrication procedure.<sup>39–43</sup>  $\gamma$ -PNA has been selected as the probe molecule due to its well-characterized binding affinity to the complementary nucleic acids, its resistance to enzymatic degradation,<sup>44,45</sup> and enhanced water solubility.<sup>46,47</sup> Furthermore, it is able to invade double-stranded DNA or RNA to form a triplex helix.<sup>48,49</sup> The device operation is based on the applied voltage and induction of electroosmotic flow across the pipet in order to direct the beads harboring miRs with low surface charge toward the sensing zone and, thus, significantly improve the sensitivity of the sensor. The probe conjugated beads serve as an intrinsic mechanical amplifier which enhance the current reduction to micro Amperes ( $\mu$ A) upon the pore blockade. As the target bead reaches the sensing zone, there is a strong opposing electrophoretic force applied on the bead resulting in a unique serrated shape electrical signal. However, in the case of the control experiments, pore blockade is permanent and the signal is right-angled in shape owing to the insufficient opposing electrophoretic force on the beads with loosely bound RNAs or no RNA.

## ■ EXPERIMENTAL SECTION

**Materials.** All chemicals were purchased from Sigma-Aldrich (St. Louis, MO) unless otherwise noted. Polyethylene glycol-amine was purchased from Nanocs Inc. (New York, NY). Borosilicate glass pipettes with an outer diameter of 1 mm and an inner diameter of 0.78 mm were purchased from Sutter Instrument (Novato, CA). A total of 0.97  $\mu$ m fluorescently tagged, carboxylic acid polystyrene beads and 2.36  $\mu$ m nonfluorescent carboxylic acid beads were acquired from Bangs Laboratories, Inc. (Fishers, IN).  $\gamma$ -PNA oligomers PNA<sub>204</sub> (amine-OOOO-GCAT\*-AGG\*-ATG\*-ACAAA), PNA<sub>210</sub> (amine-OOOO-CAGT\*-GTG\*-CGG\*-TGGGC), and NC-PNA (negative control) with noncomplementary sequences to both miR-210 and -204 (amine-OOOO-ATCA\*-AGG\*-TCC\*-GCTGT) were synthesized and purified by PNA Bio (Newbury Park, CA). MirVana microRNA Isolation Kit was purchased from Thermo Fisher Scientific Inc. (Waltham, MA).

**Beads Probe Coupling.**  $7.5 \times 10^8$  of fluorescently tagged carboxylic acid beads with 0.97  $\mu$ m diameter and  $5.1 \times 10^8$  of

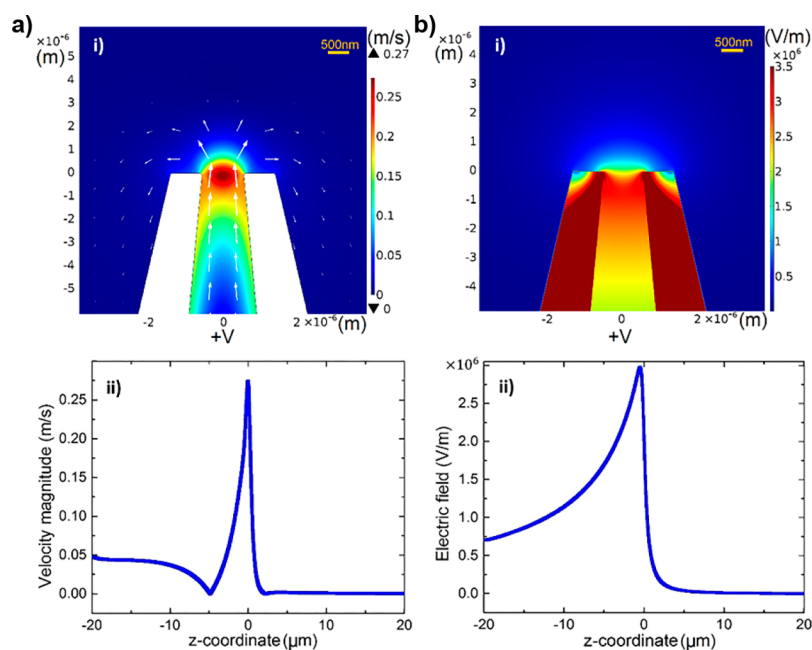
carboxylic acid beads with 2.36  $\mu$ m diameter were coupled to the amine-functionalized PNA<sub>204</sub>, PNA<sub>210</sub> and NC-PNA probes separately as described earlier.<sup>43,50</sup>

**Characterization of Beads.** Zeta potential and average diameter of the beads were measured using NanoBrook Omni (Brookhaven Instruments Corp, Holtsville, NY). The measurements of 0.97 and 2.36  $\mu$ m carboxylic acid beads were obtained to be  $-40.77 \pm 6.3$  and  $-60.63 \pm 3.7$  mV, respectively. The zeta potentials of PNA<sub>204</sub> and NC-PNA beads with 0.97  $\mu$ m diameter were measured to be  $-15.64 \pm 2.7$  and  $-11.36 \pm 6.6$  mV, respectively. The zeta potential values of PNA<sub>204</sub>, PNA<sub>210</sub>, and NC-PNA beads with 2.36  $\mu$ m diameter were  $-14.10 \pm 2.6$ ,  $-10.48 \pm 3.0$ , and  $-17.61 \pm 3.1$  mV, respectively. The average diameters of the 0.97 and 2.36  $\mu$ m beads were  $960.15 \pm 11.2$  and  $2270.05 \pm 107.0$  nm, respectively.

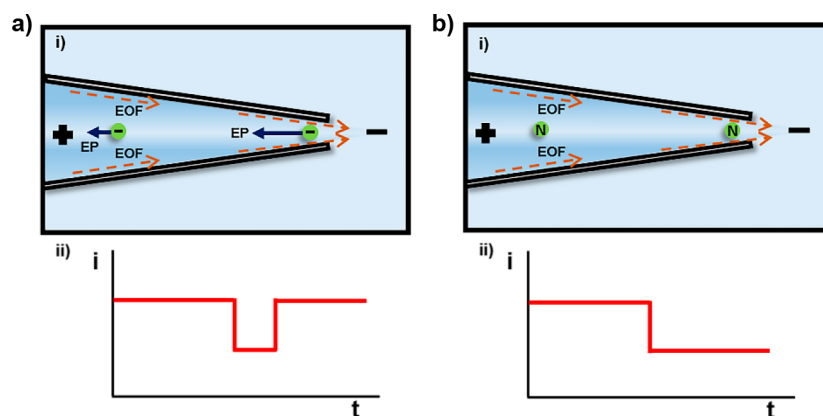
**MiRs Sample Preparation.** A total of 150000 of “786-0 Wild-Type” cells (VHL<sup>+</sup>) and “786-0 Vector” cells (VHL<sup>-</sup>) were plated on a 100 cm diameter plate in 10 mL of media containing 10% fetal bovine serum (FBS). After 3 days in culture, 1 mL of Trireagent was added to the plate to lyse the cells. Total RNAs (Kbp to 10 bp) were isolated using mirVana microRNA Isolation Kit following the provided protocol. Small RNAs (10 bp to 200 bp) were further isolated from total RNAs using the same kit and the remainder with a fraction of 200 to 1000 bp was preserved as the control NC-RNA sample. The concentration of the small RNAs extracted from the VHL<sup>+</sup> and VHL<sup>-</sup> cell lines was measured as 1.8 and 1.54  $\mu$ M, respectively; the concentration of the control NC-RNA obtained from VHL<sup>+</sup> and VHL<sup>-</sup> was measured as 16.39 and 21.5  $\mu$ M, respectively, using NanoDrop (Thermo Fisher Scientific, Waltham, MA). qRT-PCR analysis was performed to quantify the concentration of the miR-204 and miR-210 extracted from both cell lines following the established protocol by our group.<sup>38</sup> Gel electrophoresis was run to confirm the size of the small RNAs (data not shown).

**Hybridization Assay.** Prior to the hybridization reaction,  $7.5 \times 10^5$  conjugated PNA-beads were washed three times with  $0.4 \times$  SSC buffer (60 mM NaCl, 6 mM trisodium citrate, 0.1% Triton X-100 in nuclease-free water, pH 8). After the last wash, the extracted small RNA samples (containing the target miRs), and the remaining of the large RNA samples (the control NC-RNA) at serially diluted concentrations (100 mM, 1 pM, 100 fM, 10 fM, 1 fM, 0.1 fM) were incubated with different beads conjugated to different PNA probes in 50  $\mu$ L of hybridization buffer (10 mM NaCl, 25 mM Tris-HCl, pH 7.0). Hybridization reactions were performed by incubation of PNA<sub>204</sub>-beads and PNA<sub>210</sub>-beads with extracted RNA sample containing miR oligomers and control NC-RNA samples from VHL<sup>+</sup> and VHL<sup>-</sup> cells, respectively. Also, NC-PNA-beads were incubated with extracted RNA samples containing miRs from both cell lines separately. The hybridization of the PNA<sub>204</sub>-beads with small RNA extracted from VHL<sup>+</sup> cells was performed at the room temperature, while the hybridization reaction of the PNA<sub>210</sub>-beads with small RNA sample extracted from VHL<sup>-</sup> cells was performed at 50 °C. A higher melting temperature environment was set for miR-210 hybridization reaction due to its enriched Cytosine and Guanine content. After the incubation, samples were washed three times with  $0.4 \times$  SSC buffer and suspended in 1 mM KCl, pH 7.0 solution for sensing experiments.

**Sensor Apparatus and Electrical Measurements.** Micropipettes with  $\sim 1$   $\mu$ m pore diameters were fabricated by the laser-assisted puller-Sutter P2000. Borosilicate glass



**Figure 1.** Finite-element simulation by COMSOL Multiphysics: (a) Fluid flow pattern for a 1  $\mu\text{m}$  diameter pore in the near tip region with applied +30 V at the base in 1 mM KCl solution (i) and the corresponding line graph distribution along the pipet's axis (ii). (b) Nonuniform distribution of electrical field in the near tip region when +30 V is applied at the base (i) and the corresponding line graph distribution along the pipet's axis (ii).



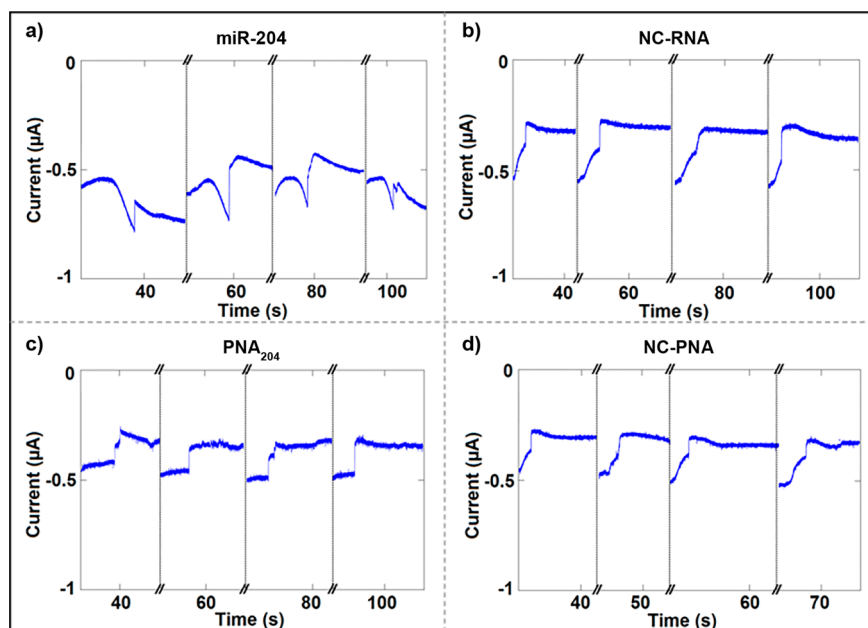
**Figure 2.** (a) (i) Schematic of electroosmotic force (EOF) and electrophoretic (EP) force applied on a negatively charged bead inside a micropipette. (ii) Depiction of a transient ionic block. (b) (i) Schematic of EOF applied on a neutral bead inside a pipet. (ii) Portrayal of a permanent ionic current reduction. Red dashed arrows represent EOF and solid blue arrows represent EP.

filament was positioned at the puller and the  $\text{CO}_2$  laser was focused into the center of the filament to melt the glass. At the end of the program, two identical pores were formed as the filament separated at the center. The programs with the following settings were used: Heat 350, Filament 4, Velocity 30, Delay 200, Pulling 0; Heat 350, Filament 4, Velocity 30, Delay 130, Pulling 30. The diameters of fabricated pores were approximated by comparison of measured conductance across the  $1\ \mu\text{m} \pm 20\%$  pipettes purchased from World Precision Instruments, Inc. (Sarasota, FL).

Two identical polydimethylsiloxane (PDMS) chambers with a 1 mm diameter opening between them were fabricated and bonded with a glass slide via Oxygen Plasma Cleaning technique (March CS-170). A micropipette was inserted into the opening and was sealed with vacuum grease to have the pipet as a sole electrical connection between the two chambers. The pipet was backfilled with an electrolyte solution (1 mM KCl and 10 mM HEPES, pH 7.0) via a 33 gauge Hamilton

syringe needle, and the two chambers were filled with  $50\ \mu\text{L}$  of electrolyte solution.

Platinum electrodes were placed into the chambers, and 30 V DC was applied using Keithley 2220G-30-1 voltage generator. The ionic current output was amplified with a homemade circuit board including a trans-impedance amplifier (OPA111). The signal was digitized by data acquisition hardware at 10 kHz sampling rate (USB 6361, National Instruments) and recorded with LabView software (National Instruments). The baseline current across the pore was stabilized and recorded for approximately 1 min prior to the injection of beads into the pipet. Beads suspended in 1 mM KCl, pH 7.0, were backfilled into the pipet, and the ionic current across the pore was recorded. The motion of the beads was simultaneously monitored and recorded using an inverted fluorescent microscope, Nikon Eclipse TE2000-E, equipped with a high-resolution camera Andor NeoZyla 5.5 at a capturing frequency of  $100\ \text{frames sec}^{-1}$ .



**Figure 3.** Detection of miR-204 oligomers from VHL+ cells. (a) Four transient ionic current blocks with unique serrated shape were obtained by PNA<sub>204</sub>-beads incubated with the extracted small RNA sample which includes miR-204 oligomers. (b) Four permanent ionic current blocks with right-angled shape were obtained by PNA<sub>204</sub>-beads incubated with control NC-RNA sample. (c) Four permanent ionic current blocks with right-angled shape were obtained by PNA<sub>204</sub>-beads in absence of RNA oligomers. (d) Four permanent ionic current blocks with right-angled shape were obtained by NC-PNA-beads incubated with small RNA samples which includes miR-204.

## RESULTS AND DISCUSSION

To design our sensor based on electroosmotically driven force, the fluid flow velocity profile and the electric field inside the pipet were simulated using the COMSOL Multiphysics (Supporting Information) with 1 mM KCl solution at pH 7.0 under 30 V (Figure 1). Figure 1a represents the fluid flow pattern of near tip region up to 6  $\mu\text{m}$  distance from the pore. The size of the arrows is proportional to the magnitude of fluid velocity and is evidently larger near the pore compared to the bulk solution. The line graph (Figure 1a(ii)) depicts the variation of surface velocity magnitude as given by the solution of Stokes equation. The variation is studied as a function of  $z$ -coordinate, which denotes the axis along the length of the channel. The negative  $z$ -coordinate pertains to the section inside of the pipet, zero implies the tip and the positive values represent the bulk of the buffer away from the tip. A sharp rise in fluid velocity can be seen at the near tip region and marked by the color gradients in the surface velocity distribution plots in Figure 1a(i).

Besides the electroosmotic flow, electrophoresis plays a crucial role on the motion of the miR:PNA-bead complex. While beads with various surface charges are driven electroosmotically toward the pore, there is a nonuniform distribution of electric field with relatively higher magnitude is induced on the negatively charged particles at the tip region (Figure 1b). Therefore, the negatively charged beads are expected to experience a strong opposing electrophoretic force (Figure 2a(i)), which is anticipated to be measured as a transient ionic current block (Figure 2a(ii)). However, the strong electric field has no effect on the beads with neutral surface charge (Figure 2b(i)); thus, a permanent current reduction is anticipated (Figure 2b(ii)).

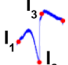
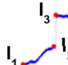
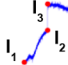
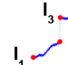
To perform the sequence-specific detection, we have targeted the miR-204 and miR-210 extracted from VHL+ and VHL- cell lines. However, this method can be expanded and used for

detection of other miRs with known sequences. Sensing experiments have been conducted after the purified small RNAs (10–200 bp) extracted from VHL+ and VHL- were hybridized with PNA<sub>204</sub>- and PNA<sub>210</sub>-beads, respectively. Three sets of control experiments were designed to investigate the selectivity of the proposed approach. The first set was performed on the noncomplementary RNA (NC-RNA), which is the remaining of the extracted total RNA after separation of the small RNAs and their incubation with PNA<sub>204</sub>- and PNA<sub>210</sub>-beads under the same hybridization conditions. The second set was the noncomplementary PNA-beads (NC-PNA-beads) incubated with the extracted small RNAs containing the target miR oligomers and the last set was of the PNA-beads with no RNA oligomers. All experiments have been performed in freshly made micropipettes and the pore blockade measurements were repeated at least 10 times by reversing the polarity of the voltage to reblock the pore with a different or the same bead. In addition to the conductance measurements, we have taken advantage of the pipet's optical transparency and simultaneously monitored the experiments optically. Figure 3 and Figure S-1 (Supporting Information) show the results of these experiments for detection of miR-204 and miR-210.

Under the applied potential, target and control beads were driven by electroosmotic flow toward the sensing zone, which resulted in pore blockades and conductance changes. The current blockades obtained by the hybridized miR-204:PNA<sub>204</sub>-beads (Figure 3a) showed a unique serrated shape compared to the right-angled shape obtained by the three control experiments (Figure 3b–d). Also, microscopic observation has shown slight backward motion of the target beads away from the tip after the initial pore blockade (Supporting Information, Video S1). However, in the case of the control experiments backward motion was unnoticeable (Supporting Information, Video S2). We have analyzed the shape of the blocks by examining four



Table 1. Current Blockades Obtained by miR-204 Detection Experiments

Current	miR-204	NC-RNA	PNA <sub>204</sub>	NC-PNA
Shape				
$I_1$ [ $\mu$ A]	-0.5103	-0.5654	-0.4334	-0.4289
$I_2$ [ $\mu$ A]	-0.6885	-0.4675	-0.3252	-0.4166
$I_3$ [ $\mu$ A]	-0.4057	-0.3181	-0.2401	-0.3471
$I_4$ [ $\mu$ A]	-0.5194	-0.3155	-0.2685	-0.3548

distinct points in current traces as a bead occluded the pore. Table 1 and Table S-1 illustrate the ionic current values at four points ( $I_1$ ,  $I_2$ ,  $I_3$ ,  $I_4$ ) in target and control experiments for detection of miR-204 and miR-210, respectively.  $I_1$  represents the open pore current,  $I_2$  and  $I_3$  declare the current drop at the moment in which the bead had blocked the pore, and  $I_4$  represents the final stable current blockade. In the case of the target experiment, the ionic current increased as beads had approached the pore ( $|I_1| < |I_2|$ ). However,  $I_2$  had decreased with respect to  $I_1$  for all three control experiments. We have postulated that the enhancement in ionic current at position 2 for beads harboring miRs is due to the particle-induced ionic concentration polarization effect,<sup>51–53</sup> in which the concentration of ions in the front region of a negatively charged bead (the right side) was enhanced while it traveled toward the cathode. However, in the case of the control beads with lower or no surface charge, the ionic current reduction was mainly due to the obstruction of the pore's opening by the particle's volume.<sup>54,55</sup> After the initial stage of the blockade, reduction of the ionic current was observed at point 3 for both target and control samples. At the tip of the pore, the negatively charged target beads were subjected to the strong opposing electrophoretic force (Figure 1b), which caused a small movement of the beads away from the tip and thus, increased the pore's conductance at point 4 ( $|I_3| < |I_4|$ ). However, in the case of the control experiments, with beads having loosely bound non-specific RNA molecules, the current reduction remained the same at points 3 and 4 ( $|I_3| \approx |I_4|$ ).

We have estimated the electrophoretic force on a 22 nt miR oligomer hybridized with the 15-mer complementary PNA probe by acquiring the electric field of  $2.97 \times 10^6$  V m<sup>-1</sup> from our simulation results (Figure 1b(ii)) near the sensing zone. The applied force was estimated as 10.45 pN (Supporting Information) which is less than  $65 \pm 15$  pN, the force required to rupture the 10 bp hybridized  $\gamma$ -PNA:DNA duplex with AFM (atomic force microscope) force spectroscopy;<sup>47</sup> and thus, the hydrogen bonds between miRs and the complementary PNA are expected to remain intact at the sensing zone. However, in the case of the control experiments the strong electric field at the tip would be sufficient to remove the weak nonspecifically bound RNAs from the bead's surface and reduce the bead's net surface charge. Therefore, the effect of the opposing electrophoretic force on the beads were diminished and the pore remained blocked under EOF.<sup>43</sup>

Furthermore, to investigate the concentration detection limit of our system, experiments were repeated as the extracted RNA samples from cell lines were diluted from 100 nM to 1 pM, 100 fM, 10 fM, 1 fM, and 0.1 fM and hybridized with the corresponding target and control PNA-beads. The current blocks by the miR-204:PNA-beads were observed as transient with the signature serrated shape (Figure 4a), while permanent

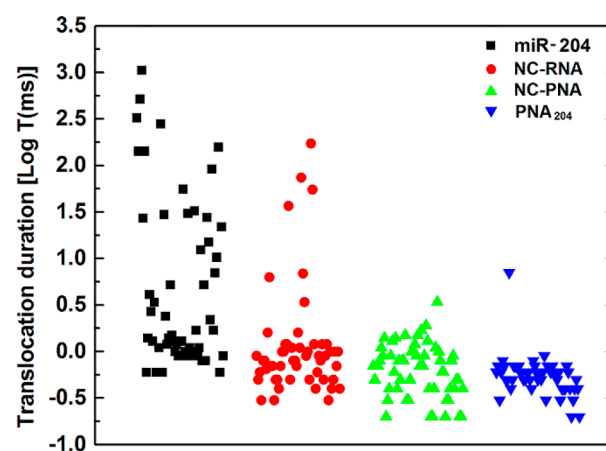

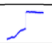






Figure 4. Scatter plot of translocation events of 0.97  $\mu$ m beads through a 1  $\mu$ m pore for detection of miR-204 extracted from VHL+ cells: (a) translocation of 55 PNA<sub>204</sub>-beads incubated with 60 nM small RNA sample, which includes miR-204 oligomers; (b) translocation of 53 PNA<sub>204</sub> beads incubated with 60 nM control NC-RNA sample; (c) translocation of 57 NC-PNA-beads incubated with 60 nM small RNA sample, which includes miR-204; (d) translocation of 53 PNA<sub>204</sub>-beads in the absence of RNA oligomers. The translocation time presented at the Y-axis was taken as  $\log(T)$ , in which  $T$ /ms is the dwelling time of each bead passing through the pore.

current blockades with right-angled shape were obtained in the control experiments (Figure 4b,d). The number of serrated shapes were counted at each dilution for both target and control experiments (Table 2). As the concentration of the RNA decreased to 0.1 fM, more right-angled blocks were obtained which indicates that the limit of detection (LOD) of our system is 1 fM for miR-204.

Similar experiments were repeated for detection of miR-210 as described above. As the RNA concentration decreased to 1 fM, the majority of the blockades were detected as right-angled shape, which indicates the LOD of the system as 10 fM for

Table 2. LOD of the System for Detection of miR-204

Concentration	miR-204		NC-RNA		NC-PNA	
						
100 [nM]	22	1	5	16	0	19
1 [pM]	18	0	0	23	0	22
100 [fM]	11	0	0	18	0	23
10 [fM]	13	0	0	33	0	23
1 [fM]	11	1	0	17	0	17
0.1 [fM]	2	20	0	21	0	21

miR-210 (Table S-2). In addition, out of 137 blocks obtained in 33 target experiments at different concentrations, we have counted the number of the right-angled blocks and have estimated a “false negative” rate of 2.2% for our system. Moreover, by counting the number of the serrated shape blockades out of 364 blocks obtained in 54 control experiments, we have estimated a “false positive” rate of 2.5% for our system. Overall, the accuracy of our device is estimated as 97.6%. However, we have noticed a fairly large percentage of false positive  $\sim 21.6\%$ , in the case of the control NC-RNA experiment at 100 nM which could be the result of the large number of nonspecifically bound RNAs to the beads’ surface at higher concentration and an indication of our system’s upper detection limit.

To further support our results, we have repeated the miR-204 detection experiments at 60 nM with  $0.97\ \mu\text{m}$  beads translocating through a  $1\ \mu\text{m}$  pore using the electroosmotic flow as the driving force and analyzed the duration of the resistive pulses. Recently, zeta potential of particles has been accurately estimated utilizing a nanopore device in which the electrophoretic mobility of the particle is calculated based on the particle’s translocation velocity through the pore.<sup>56,57</sup> We have followed the same concept to investigate the correlation between the particle’s translocation velocity and its surface charge. In these experiments, longer translocation time (“dwelling time”) for beads harboring miR-204 with higher surface charge density has been observed compared to the control beads with lower surface charge (Figure 4). Supporting Information Videos S3 and S4 illustrate the microscopic observation of the target and control beads through a pore. According to the scatter plot, a wide distribution of dwelling time for the target beads was observed, which could be interpreted as (1) the particles have nonuniform coating of PNA probes on their surface<sup>57</sup> and (2) the hybridization between PNA probes and miRs followed a Gaussian distribution, which leads to a distribution of beads with various surface charges.<sup>58,59</sup> The average dwelling time of 55 beads harboring target miR-204 was approximately 55.31 ms, which was significantly longer than the average dwelling time of approximately the same number of beads in the three control experiments. The average dwelling time of the control NC-RNA incubated with PNA<sub>204</sub>-beads and NC-PNA-beads incubated with the small RNA oligomers was measured as  $\sim 7.39$  and  $\sim 0.77$  ms, respectively. For PNA<sub>204</sub>-beads in the absence of RNA oligomers, the average translocation velocity was recorded as  $\sim 0.90$  ms. The longer translocation time for the target beads confirmed the effect of the opposing electrophoretic force on the negatively charged particles which resulted in the reduction of their electroosmotic velocity. The shorter translocation time for the control beads validates our argument regarding the dissociation of weakly bound RNAs under the strong electric field at the tip, and their fast translocation through the pore under the EOF. Interestingly, the average dwelling time of the beads in the NC-PNA experiment is in-between the translocation velocity of the PNA<sub>204</sub> and the control NC-RNA experiments. This observation can be explained by evaluating the length of the RNA oligomers that could have been nonspecifically bound to the beads. In the case of the NC-PNA-beads incubated with the extracted small RNA samples, the lengths of the oligonucleotides were in the range of 10–200 bp. However, in the case of PNA<sub>204</sub>-beads incubated with the control NC-RNAs, the length of the oligonucleotides was 200–1000 bp, which resulted in

their slower translocation time. Also, the long dwelling time of the control NC-RNA experiment was in agreement with the high “false positive” rate of the same experiment with  $2.36\ \mu\text{m}$  beads at 100 nM as described above. Overall, the resistive pulse results support the blockade experiments, which validate the influence of the opposing electrophoretic force on the negatively charged beads and thus their slower translocation velocity through the pore compared to the control beads.

## CONCLUSION

We have elucidated a sensitive and robust nanopore-based sensing scheme which took advantage of the electroosmotic flow inside a conical glass micropipette and highly specific  $\gamma$ -PNA probes conjugated beads, to accurately detect miR-204 and miR-210 fragments against the small RNA background. Detection results exhibited a high accuracy of our sensor with 97.6% in 87 experiments. The limit of detection for miR-204 and miR-210 were demonstrated as 1 and 10 fM, respectively. Moreover, analysis of the dwelling times of resistive pulses was performed to validate the measured signature serrated shape signals obtained by the target samples in our blockade experiments. This sensitive scheme can be applied for detection of all miR oligomers with known sequences by designing the specific  $\gamma$ -PNA probes complementary to the target miR sequences. Furthermore, the proposed sensor has a technological appeal to be evolved into a quantitative measurement tool for analysis of miR biomarkers in basic and clinical research by correlating the dwelling time of particles with the concentration of the RNA oligomers bound to their surface.

## ASSOCIATED CONTENT

### Supporting Information

Videos: Four videos regarding beads’ electrohydrodynamic trajectories inside of  $1\ \mu\text{m}$  borosilicate micropipettes. The Supporting Information is available free of charge on the ACS Publications website at DOI: 10.1021/acs.analchem.7b01944.

Finite element modeling of the nanopore: COMSOL simulation of electric field and fluid velocity inside of the nanopore. Figure S-1: Detection of miR-210 oligomers from VHL– cells. Table S-1: Current blockades obtained by miR-210 detection experiments. Table S-2: The LOD of the system for detection of miR-204. Force estimation: Calculation of electrophoretic force exerted on an oligomer (PDF).

Video S1 Target: miR-204 target experiment with  $2.36\ \mu\text{m}$  diameter beads and  $1\ \mu\text{m}$  pore. Video recording of miR-204:PNA204 beads motion in 1mM KCl (pH 7.0) under 30 V bias (polarity was marked in the video). The clip shows a bead harboring miR-204 moved toward the negative polarity and oscillated at the pipette’s tip. As the voltage polarity had been reversed, the bead moved backwards away from the pore (AVI).

Video S2 Control: PNA204 conjugated to the  $2.36\ \mu\text{m}$  diameter beads and  $1\ \mu\text{m}$  pore. Video recording of PNA204 conjugated beads with low surface charge ( $-14.1 \pm 2.65$  mV) in 1 mM KCl (pH 7) under 30 V bias (polarity was noted in the video). The clip shows a PNA conjugated bead had moved toward the negative polarity and blocked the pore; by reversing the voltage polarity the pore became open (AVI).

Video S3 Target: miR-204 target experiments with  $0.97\ \mu\text{m}$  diameter beads and  $1\ \mu\text{m}$  pore. Video recording of

miR-204:PNA204 beads in 1mM KCl (pH 7) under 30V bias (polarity was marked in the video). The clip shows the beads harboring miR-204 had moved toward the tip and stopped around 500 ms at the tip before passing through the pore (AVI).

Video S4 Control: PNA204 conjugated to the 0.97  $\mu\text{m}$  diameter beads and 1  $\mu\text{m}$  pore. Video recording of PNA204 conjugated beads in 1 mM KCl (pH 7) under 30 V bias (polarity was marked in the video). Beads had moved toward the tip and passed through the pore with high velocity (AVI).

## AUTHOR INFORMATION

### Corresponding Author

\*E-mail: [esfandla@ucmail.uc.edu](mailto:esfandla@ucmail.uc.edu). Fax: 513-556-7326.

### ORCID

Yuqian Zhang: 0000-0002-2800-6100

Ankit Rana: 0000-0002-9866-9620

Leyla Esfandiari: 0000-0001-6851-1198

### Notes

The authors declare no competing financial interest.

## ACKNOWLEDGMENTS

This work was funded by UC College of Engineering start-up funds to L.E. M.F.C.-K. was supported by R01 NCI CA 122341 and VA Merit Award 2101BX001110-05A1. The authors thank Dr. S. Chae and his group members for valuable assistance with the Dynamic Light Scattering measurements. We also thank members of M.F.C.-K.'s group, especially M. Bischoff, for generously providing 786-0 cell lines.

## REFERENCES

- Huang, Y.; Shen, X. J.; Zou, Q.; Wang, S. P.; Tang, S. M.; Zhang, G. Z. *J. Physiol. Biochem.* **2011**, *67*, 129–139.
- Kim, V. N.; Han, J.; Siomi, M. C. *Nat. Rev. Mol. Cell Biol.* **2009**, *10*, 126–139.
- Croce, C. M. *Nat. Rev. Genet.* **2009**, *10*, 704–714.
- Davalos, V.; Esteller, M. *Curr. Opin. Oncol.* **2010**, *22*, 35–45.
- Hunter, M. P.; Ismail, N.; Zhang, X.; Aguda, B. D.; Lee, E. J.; Yu, L.; Xiao, T.; Schafer, J.; Lee, M.-L. T.; Schmittgen, T. D. *PLoS One* **2008**, *3*, e3694.
- Valenti, R.; Huber, V.; Iero, M.; Filipazzi, P.; Parmiani, G.; Rivoltini, L. *Cancer Res.* **2007**, *67*, 2912–2915.
- Taylor, D. D.; Gercel-Taylor, C. *Semin. Immunopathol.*; Springer, 2011; pp 441–454.
- Chen, X.; Ba, Y.; Ma, L.; Cai, X.; Yin, Y.; Wang, K.; Guo, J.; Zhang, Y.; Chen, J.; Guo, X. *Cell Res.* **2008**, *18*, 997–1006.
- Iwamoto, H.; Kanda, Y.; Sejima, T.; Osaki, M.; Okada, F.; Takenaka, A. *Int. J. Oncol.* **2014**, *44*, 53–58.
- Madhavan, D.; Cuk, K.; Burwinkel, B.; Yang, R. *Front. Genet.* **2013**, *4*, 116.
- Chen, C.; Ridzon, D. A.; Broomer, A. J.; Zhou, Z.; Lee, D. H.; Nguyen, J. T.; Barbisin, M.; Xu, N. L.; Mahuvakar, V. R.; Andersen, M. R. *Nucleic Acids Res.* **2005**, *33*, e179–e179.
- Lao, K.; Xu, N. L.; Yeung, V.; Chen, C.; Livak, K. J.; Straus, N. A. *Biochem. Biophys. Res. Commun.* **2006**, *343*, 85–89.
- Murphy, J.; Bustin, S. A. *Expert Rev. Mol. Diagn.* **2009**, *9*, 187–197.
- Li, W.; Ruan, K. *Anal. Bioanal. Chem.* **2009**, *394*, 1117–1124.
- Zhang, G.-J.; Chua, J. H.; Chee, R.-E.; Agarwal, A.; Wong, S. M. *Biosens. Bioelectron.* **2009**, *24*, 2504–2508.
- Lusi, E.; Passamano, M.; Guarascio, P.; Scarpa, A.; Schiavo, L. *Anal. Chem.* **2009**, *81*, 2819–2822.
- Wu, X.; Chai, Y.; Yuan, R.; Su, H.; Han, J. *Analyst* **2013**, *138*, 1060–1066.
- Fang, S.; Lee, H. J.; Wark, A. W.; Corn, R. M. *J. Am. Chem. Soc.* **2006**, *128*, 14044–14046.
- Wegman, D. W.; Krylov, S. N. *Angew. Chem.* **2011**, *123*, 10519–10523.
- Yildiz, U. H.; Alagappan, P.; Liedberg, B. *Anal. Chem.* **2013**, *85*, 820–824.
- Johnson, B. N.; Mutharasan, R. *Analyst* **2014**, *139*, 1576–1588.
- Deamer, D. W.; Akeson, M. *Trends Biotechnol.* **2000**, *18*, 147–151.
- Astier, Y.; Braha, O.; Bayley, H. *Science* **2005**, *309*, 1728–1732.
- Atas, E.; Singer, A.; Meller, A. *Electrophoresis* **2012**, *33*, 3437–3447.
- Haque, F.; Li, J.; Wu, H.-C.; Liang, X.-J.; Guo, P. *Nano Today* **2013**, *8*, 56–74.
- Fahie, M. A.; Yang, B.; Mullis, M.; Holden, M. A.; Chen, M. *Anal. Chem.* **2015**, *87*, 11143–11149.
- Heins, E. A.; Siwy, Z. S.; Baker, L. A.; Martin, C. R. *Nano Lett.* **2005**, *5*, 1824–1829.
- Liu, A.; Zhao, Q.; Guan, X. *Anal. Chim. Acta* **2010**, *675*, 106–115.
- Garaj, S.; Hubbard, W.; Reina, A.; Kong, J.; Branton, D.; Golovchenko, J. *Nature* **2010**, *467*, 190–193.
- Gu, L.-Q.; Wanunu, M.; Wang, M. X.; McReynolds, L.; Wang, Y. *Expert Rev. Mol. Diagn.* **2012**, *12*, 573–584.
- Tian, K.; He, Z.; Wang, Y.; Chen, S.-J.; Gu, L.-Q. *ACS Nano* **2013**, *7*, 3962–3969.
- Wang, Y.; Zheng, D.; Tan, Q.; Wang, M. X.; Gu, L.-Q. *Nat. Nanotechnol.* **2011**, *6*, 668–674.
- Zhang, X.; Wang, Y.; Fricke, B. L.; Gu, L.-Q. *ACS Nano* **2014**, *8*, 3444–3450.
- Wanunu, M.; Dadosh, T.; Ray, V.; Jin, J.; McReynolds, L.; Drndić, M. *Nat. Nanotechnol.* **2010**, *5*, 807–814.
- Gossage, L.; Eisen, T. *Nat. Rev. Clin. Oncol.* **2010**, *7*, 277–288.
- Redova, M.; Poprach, A.; Besse, A.; Iliev, R.; Nekvindova, J.; Lakomy, R.; Radova, L.; Svoboda, M.; Dolezel, J.; Vyzula, R. *Tumor Biol.* **2013**, *34*, 481–491.
- Hall, D. P.; Cost, N. G.; Hegde, S.; Kellner, E.; Mikhaylova, O.; Stratton, Y.; Ehmer, B.; Abplanalp, W. A.; Pandey, R.; Biesiada, J. *Cancer Cell* **2014**, *26*, 738–753.
- Mikhaylova, O.; Stratton, Y.; Hall, D.; Kellner, E.; Ehmer, B.; Drew, A. F.; Gallo, C. A.; Plas, D. R.; Biesiada, J.; Meller, J. *Cancer Cell* **2012**, *21*, 532–546.
- Fu, Y.; Tokuhisa, H.; Baker, L. A. *Chem. Commun.* **2009**, 4877–4879.
- Bell, N. A.; Keyser, U. F. *J. Am. Chem. Soc.* **2015**, *137*, 2035–2041.
- Li, W.; Bell, N. A.; Hernández-Ainsa, S.; Thacker, V. V.; Thackray, A. M.; Bujdosó, R.; Keyser, U. F. *ACS Nano* **2013**, *7*, 4129–4134.
- Zhang, Y.; Edwards, M. A.; German, S. R.; White, H. S. *J. Phys. Chem. C* **2016**, *120*, 20781–20788.
- Esfandiari, L.; Monbouquette, H. G.; Schmidt, J. J. *J. Am. Chem. Soc.* **2012**, *134*, 15880–15886.
- Pellestor, F.; Paulasova, P.; Hamamah, S. *Curr. Pharm. Des.* **2008**, *14*, 2439–2444.
- Zhang, N.; Appella, D. H. *J. Am. Chem. Soc.* **2007**, *129*, 8424–8425.
- Englund, E. A.; Appella, D. H. *Angew. Chem., Int. Ed.* **2007**, *46*, 1414–1418.
- Dutta, S.; Armitage, B. A.; Lyubchenko, Y. L. *Biochemistry* **2016**, *55*, 1523–1528.
- Hansen, M. E.; Bentin, T.; Nielsen, P. E. *Nucleic Acids Res.* **2009**, *37*, 4498–4507.
- Avitabile, C.; Moggio, L.; Malgieri, G.; Capasso, D.; Di Gaetano, S.; Saviano, M.; Pedone, C.; Romanelli, A. *PLoS One* **2012**, *7*, e35774.
- Esfandiari, L.; Lorenzini, M.; Kocharyan, G.; Monbouquette, H. G.; Schmidt, J. J. *Anal. Chem.* **2014**, *86*, 9638–9643.

- (51) Chang, H.; Kosari, F.; Andreadakis, G.; Alam, M.; Vasmatzis, G.; Bashir, R. *Nano Lett.* **2004**, *4*, 1551–1556.
- (52) Yeh, L.-H.; Zhang, M.; Qian, S.; Hsu, J.-P.; Tseng, S. *J. Phys. Chem. C* **2012**, *116*, 8672–8677.
- (53) Qiu, Y.; Lin, C.-Y.; Hinkle, P.; Plett, T. S.; Yang, C.; Chacko, J. V.; Digman, M. A.; Yeh, L.-H.; Hsu, J.-P.; Siwy, Z. S. *ACS Nano* **2016**, *10*, 8413–8422.
- (54) Smeets, R. M.; Keyser, U. F.; Krapf, D.; Wu, M.-Y.; Dekker, N. H.; Dekker, C. *Nano Lett.* **2006**, *6*, 89–95.
- (55) Howorka, S.; Siwy, Z. *Chem. Soc. Rev.* **2009**, *38*, 2360–2384.
- (56) Arjmandi, N.; Van Roy, W.; Lagae, L.; Borghs, G. *Anal. Chem.* **2012**, *84*, 8490–8496.
- (57) Blundell, E. L.; Vogel, R.; Platt, M. *Langmuir* **2016**, *32*, 1082–1090.
- (58) Mullen, D. G.; Fang, M.; Desai, A.; Baker, J. R., Jr; Orr, B. G.; Banaszak Holl, M. M. *ACS Nano* **2010**, *4*, 657–670.
- (59) Uddayasankar, U.; Shergill, R. T.; Krull, U. J. *Anal. Chem.* **2015**, *87*, 1297–1305.